ELECTRICAL CONDUCTIVITY AND TENSILE PROPERTIES OF COPPER AND OXIDE DISPERSION STRENGTHENED COPPER ALLOYS FOLLOWING HFIR IRRADIATION TO 13 DPA AT 200 AND 400°C – S. J. Zinkle and L. T. Gibson (Oak Ridge National Laboratory)

OBJECTIVE

The objective of this report is to summarize recent tensile and electrical resistivity measurements on pure copper and oxide dispersion strengthened copper alloys following HFIR irradiation to ~13 dpa at 200 and 400°C

SUMMARY

The tensile properties and room temperature electrical resistivity have been measured for pure copper and MAGT 0.2, GlidCop AL15 and GlidCop AL25 oxide dispersion strengthened copper alloys following irradiation in the spectrally tailored HFIR-MFE-200J and –400J irradiation capsules. The tensile measurements were performed at the irradiation temperature and at room temperature, at strain rates between $2x10^{-5}$ s^{-1} and 0.01 s^{-1}. Significant increases in the tensile strength were observed following irradiation at 200°C, accompanied by a reduction in uniform elongation. The irradiation at 400°C had only a moderate effect on the tensile properties. A large increase in the electrical resistivity (mainly attributable to solid solution transmutation products) was observed for both irradiation temperatures. The tensile strength increased with increasing strain rate, particularly for the GlidCop Al25 alloys irradiated and tested at 400°C. The effect of test temperature on the yield and ultimate strengths was much more pronounced in the irradiated GlidCop specimens compared to the unirradiated specimens.

PROGRESS AND STATUS

Introduction

High-strength, high-conductivity copper alloys are being considered for first wall heat sink and divertor structural applications in fusion energy systems such as the proposed International Thermonuclear Experimental Reactor (ITER) [1-3]. Copper alloys have also been proposed for the centerpost magnet in spherical tokamaks. Although a considerable amount of high fluence microstructural and room temperature tensile data exist for copper alloys irradiated at temperatures above ~380°C [1,4-6], there are only a few high dose (>1 dpa) studies on copper irradiated at lower temperatures. The main radiation effects which occur in copper alloys at 200-400°C are radiation hardening (with accompanying embrittlement) and void swelling. Low dose (<1 dpa) studies of copper irradiated at temperatures ≤200°C suggest that the amount of radiation hardening approaches saturation for damage levels above ~0.1 dpa. One of the objectives of the present study was to determine whether this apparent hardening saturation is maintained up to damage levels in excess of 10 dpa.

Experimental Procedure

A limited amount of space was allocated to copper alloy specimens in the HFIR-MFE-200J and –400J irradiation capsules. Based on the promising radiation resistance obtained in prior high-dose irradiation studies in FFTF [1,4-6], the HFIR matrix placed a heavy emphasis on dispersion strengthened copper alloys (GlidCop and MAGT alloys). Several of the specimen heats were identical to those used in prior irradiation experiments in order to facilitate comparisons. Pure

copper was also included as a reference material. The GlidCop Al15 and Al25 alloys contained 0.15 wt.% and 0.25 wt.% Al, respectively, in the form of small aluminum oxide particles. The B-deoxidized GlidCop alloys contained ~0.01 wt.%B. The MAGT 0.2 alloys had a chemical composition of Cu-0.2%Al-0.05%Hf-0.05%Ti-0.2%O, and consisted of a pure copper matrix with small oxide particles [7]. GlidCop Al15 induction brazed sheet tensile specimens were machined from a brazed bar such that the braze joint was located in the center of the gage region (butt joint configuration). These specimens were brazed with a Cu-6%P-5%Ag alloy at 810°C for 81 s in a Gleeble resistance-heating machine. Both type SS1 and SS3 miniature sheet tensile specimens were included in the irradiation capsules (nominal gage dimensions of 1.52x0.76x20.3 mm and 1.52x0.76x7.6 mm, respectively). The 80% cold-rolled GlidCop Al25 +B tensile specimens had a nominal thickness of 0.51 mm. The gage dimensions of all of the individual specimens were measured prior to irradiation. All of the specimens were electroplated with a 5-10 μm layer of Ni prior to irradiation in order to minimize diffusion bonding of the copper specimens during the irradiation.

The specimens were loaded in the Hf spectrally shielded HFIR-MFE-200J and –400J capsules, which operated for 440.6 effective full power days in the Removable Beryllium irradiation positions of HFIR [8,9]. The detailed specimen matrix (including TEM disks) for the irradiation capsules is described elsewhere [10]. Most of the Cu alloy tensile specimens were located in the top half of the two irradiation capsules. The fast neutron fluence in the capsules ranged from 1.36 to 1.94×10^{26} n/m^2-s, which corresponds to 10.4 to 14.9 dpa in copper [9]. The 4.2 mm hafnium shielding reduced the horizontal midplane thermal neutron flux to 9.2×10^{18} n/m^2-s, which is ~20% of its normal value. The calculated dominant solute transmutations in copper were 1.4% Ni and 0.5% Zn. The irradiation produced a calculated He concentration of 2 appm in pure copper. Higher levels of helium (up to ~100 appm) should have been produced in the boron-deoxidized GlidCop specimens. The average irradiation temperatures of the 200J and 200J capsules were maintained at 200 and 400°C, respectively. The detailed operating temperature history is given in ref. [8].

Four-point probe electrical resistivity measurements were performed at room temperature on the irradiated SS-1 and SS-3 sheet tensile specimens, using procedures summarized elsewhere [11]. The temperature was recorded for each measurement and the resistivity data were corrected to a reference temperature of 20°C using the copper resistivity temperature coefficient of $d\rho/dT = 6.7 \times 10^{-11}$ Ω-m/K. Nonuniformities in the width and thickness in the specimen gage region caused the typical experimental uncertainty of individual resistivity measurements to be ±0.5%. The resistivity data were corrected for the influence of the Ni plating, which amounted to an ~2% change compared to the raw data.

All of the tensile specimens were tested in a hot cell using a 200 pound load cell mounted on a screw-driven Instron machine. Table 1 summarizes the tensile specimen experimental matrix. Several specimens were broken (specimens C2, F3 and X1 from HFIR-200J and A11 from HFIR-400J) or bent during capsule disassembly (cf. Table 1). The induction brazed specimen F4 (HFIR-400J) broke during mounting for tensile testing in the hot cells. Specimen L8 from HFIR-400J was severely bent and was not tested. Specimens W3, T1 and X3 from HFIR-200J and H5, L7 from HFIR-400J were also significantly deformed during capsule disassembly such that valid tensile data could not be obtained. Strain rate variation tests were performed on some specimens, including several of the bent specimens in order to measure the strain rate sensitivity of the radiation hardened samples. The crosshead speed was varied from 0.001 to 0.5 inch per minute, which resulted in strain rates of 2×10^{-5} to 0.01 s^{-1}. The room temperature tests were performed in air, and the elevated temperature tests were performed in vacuum (<10^{-5} torr). The samples were held at the test temperature for 15 minutes prior to testing.

Table 1. Specimen matrix and tensile test conditions for the pure copper and GlidCop dispersion strengthened copper alloys irradiated in the HFIR-200J and –400J capsules. The specimens with ID code in parentheses were bent during capsule disassembly.

SS-1 and SS-3 specimens from HFIR-MFE-RB*-200J-1 capsule

Alloy	Geometry	ID code	Test temperature & crosshead speed
99.999% copper, as wrought (MRC Marz grade rod)	SS-1	A6 A8 (A7)	200°C, 0.02"/min 29°C, 0.02"/min 200°C, 0.001"/min through 0.2% yield, then increase to 0.02"/min
GlidCop AL15+B, as wrought (ORNL plate)	SS-1	L1 L2 L3	200°C, 0.5"/min 200°C, 0.001"/min 200°C, 0.02"/min
GlidCop AL25, as wrought (Risø rod, no boron)	SS-1	H2 H3 (H1)	200°C, 0.02"/min 29°C, 0.02"/min 200°C, 0.001"/min through 0.2% yield, then increase to 0.02"/min
GlidCop AL25, 50%CW (PNL "R4" 40 mil sheet)	SS-3	X2 (X3)	200°C, 0.02"/min 200°C, 0.001"/min through 0.2% yield, then increase to 0.02"/min
GlidCop AL25+B (Risø), 80% CW, 0.02" thick (626AAF, lot #4005m09)	SS-3	C1 C3	200°C, 0.02"/min 200°C, 0.001"/min
GlidCop AL25+B (Risø), as-wrought (616 AAE, lot #4005806 rod)	SS-3	W1 W2 (W3)	200°C, 0.02"/min 20°C, 0.02"/min 200°C, 0.001"/min through 0.2% yield, then increase to 0.02"/min
MAGT 0.2, 50%CW (Technology 1)	SS-3	T2 T3 (T1)	200°C, 0.02"/min 200°C, 0.02"/min 200°C, 0.001"/min through 0.2% yield, then increase to 0.02"/min
GlidCop AL15+B, Auburn U. induction brazed (ORNL as-wrought plate)	SS-3	F1 F2	200°C, 0.02"/min 29°C, 0.02"/min

Table 1, continued: SS-1 and SS-3 specimens from HFIR-MFE-RB*-400J-1 capsule.

Alloy	Geometry	ID code	Test temperature & crosshead speed
99.999% copper, as wrought (MRC Marz grade rod)	SS-1	(A09) (A10)	400°C, 0.02"/min 29°C, 0.02"/min
GlidCop AL15+B, as wrought (ORNL plate)	SS-1	L06 (L07)	400°C, 0.02"/min 400°C, 0.02"/min
GlidCop AL25, as wrought (Risø rod, no boron)	SS-1	H04 H06 (H05)	400°C, 0.02"/min 30°C, 0.02"/min 400°C, 0.001"/min through 0.2% yield, then increase to 0.02"/min
GlidCop AL25, 50%CW (PNL "R4" 40 mil sheet)	SS-3	X4 X5 X6	400°C, 0.02"/min; 30°C, 0.02"/min; 400°C, 0.001"/min through 0.2% yield, then increase to 0.02"/min
GlidCop AL25+B (Risø), 80% CW, 0.02" thick (626AAF, lot #4005m09)	SS-3	C6 C7 C8	400°C, 0.02"/min; 400°C, 0.001"/min; 30°C, 0.02"/min
GlidCop AL25+B (Risø), as-wrought (616 AAE, lot #4005806 rod)	SS-3	W4 W5 W6	400°C, 0.02"/min; 400°C, 0.02"/min; 30°C, 0.02"/min
MAGT 0.2, 50%CW (Technology 1)	SS-3	T4 T5 T6	400°C, 0.02"/min; 30°C, 0.02"/min; 400°C, 0.001"/min through 0.2% yield, then increase to 0.02"/min
GlidCop AL15+B, Auburn U. induction brazed (ORNL as-wrought plate)	SS-3	F5 F6	400°C, 0.02"/min; 30°C, 0.02"/min

Results and Discussion

The electrical resistivity measurements on the unirradiated and irradiated specimens are summarized in Table 2. A large variability was obtained for the resistivity of the unirradiated induction-brazed GlidCop Al15 specimens, presumably due to variations in the thickness of the braze layer. The resistivity of the unirradiated pure copper and dispersion-strengthened copper alloys were in agreement with data obtained on other heats of these materials [12-16]. The increase in resistivity for most of the copper alloys in both the 200J and 400J capsules was ~6 to 8 nΩ-m. Previous work has found that the resistivity increase associated with defect cluster (stacking fault tetrahedra, small dislocation loops) formation in copper saturates at ~1.2 nΩ-m [13]. The remaining 5-7 nΩ-m resistivity increase for the HFIR-200J specimens can be attributed to Ni, Zn, Co solid transmutation products, since transmission electron microscopy (TEM) did not find evidence for void formation in Cu and Cu alloy specimens in this capsule [17]. The resistivity of the as-wrought GlidCop Al25+B specimens irradiated in the HFIR-400J capsule were anomalously high for unknown reasons. The resistivity of the specimens in the HFIR-400J capsule was generally higher than that of the HFIR-200J capsule. TEM investigation did not detect void formation in GlidCop Al25, whereas a moderate density of large cavities was observed in pure copper irradiated in the HFIR-400J capsule [17].

Table 2. Summary of electrical resistivity measurements on the pure copper and GlidCop dispersion strengthened copper alloy specimens from HFIR-MFE-200J and –400J capsules.

Alloy, ID number	Unirrad. resistivity (nΩ-m)	Resistivity of specimens irrad. at 200°C (nΩ-m)	Resistivity of specimens irrad. at 400°C (nΩ-m)
pure copper, as wrought (SS1)	17.18±0.11	23.40±0.16	23.61 (1 spec.)
GlidCop AL15+B, as wr't (SS1)	18.79±0.12	27.36±0.32	25.38±0.22
GlidCop AL25, as wrought (SS1)	19.26±0.08	26.38±0.18	29.59±1.4
GlidCop AL25, 50%CW (SS3)	19.40±0.16	26.52±0.70	27.75±1.28
GlidCop AL25+B, 80% CW (SS3)	19.35±0.07	26.20±0.07	28.56±1.61
GlidCop AL25+B, as-wr't (SS3)	19.42±0.15	25.93±0.25	35.32±0.35
MAGT 0.2, 50%CW (SS3)	21.91±0.08	27.47±0.05	29.28±0.24
GlidCop AL15+B, induction brazed (SS3)	25.5±3.1	27.06±0.50	27.02±0.78

Tables 3 and 4 summarize the tensile data obtained on the specimens from the HFIR-200J and –400J capsules, respectively. The strain hardening capacity of the irradiated specimens was low in all specimens tested at the irradiation temperature, with typical uniform elongation values of ~1%. Irradiation at 200°C produced a 100-150 MPa increase in the room temperature yield strength of the GlidCop dispersion strengthened copper alloys, and a ~200 MPa increase in the room temperature yield strength of pure copper. Figure 1 plots the room temperature yield strength of copper (specimen A8) along with previous low temperature (20-150°C) results on pure copper [18-24]. The results suggest that saturation in the radiation hardening occurs for doses above ~0.1 dpa, although the influence of the higher irradiation temperature of the HFIR-200J experiment (200°C) compared to the other experiments summarized in Fig. 1 (20-150°C) needs further investigation.

Table 3. Tensile test results on copper alloy specimens from HFIR-MFE-200J capsule. The tensile data in parentheses are considered unreliable due to bent or brittle tensile specimens.

Alloy, ID number	Temperature (°C)	Strain rate (s^{-1})	Yield Strength (MPa)	Ultimate Strength (MPa)	Uniform Elong. (%)	Total Elong. (%)
Marz copper, as wrought						
A6 (SS1)	200	4.2×10^{-4}	239	242	1.1	7.7
A8 (SS1)	29	4.2×10^{-4}	306	308	2.2 (stn)[a]	7.1
A7 (SS1)-sharp bend	200	$0.21\text{->}4.2\times10^{-4}$	($\Delta\sigma$~3.5)	–	–	–
GlidCop AL25, as wrought						
H2 (SS1)	200	4.2×10^{-4}	430	445	0.5	7.2
H3 (SS1)	30	4.2×10^{-4}	529	560	0.7	3.8
H1 (SS1)-bent/twisted	200	$0.21\text{->}4.2\times10^{-4}$	($\Delta\sigma$~7)	–	–	–
GlidCop AL15+B, as wr't						
L1 (SS1)	200	0.010	461	475	0.6	2.2
L2 (SS1)	200	2.1×10^{-5}	402	406	0.4	1.7
L3 (SS1)	200	4.2×10^{-4}	431	433	0.3	1.2
GlidCop AL25, 50%CW						
X2 (SS3)	200	1.1×10^{-3}	490	524	0.8	2.8
X3 (SS3)-bent	200	$0.56\text{->}11\times10^{-4}$	$\Delta\sigma$~11	–	–	–
GlidCop AL25+B, 80% CW						
C1 (SS3)	200	1.1×10^{-3}	575	580	0.4	1.9
C3 (SS3)	200	5.6×10^{-5}	530	549	0.5	2.2
GlidCop AL25+B, as-wr't						
W1 (SS3)	200	1.1×10^{-3}	471	490	0.5	8.3
W2 (SS3)	29	1.1×10^{-3}	569	601	0.5	6.7
W3 (SS3)-bent sample	200	$0.56\text{->}11\times10^{-4}$	$\Delta\sigma$=17		–	–
MAGT 0.2, 50%CW						
T2 (SS3)	200	1.1×10^{-3}	497	523	0.7	4.8
T3 (SS3)	200	1.1×10^{-3}	477	499	0.7	4.7
T1 (SS3)-bent	200	$0.56\text{->}11\times10^{-4}$	$\Delta\sigma$=16.5	(495/512)	–	–
GlidCop AL15+B, ind. braze						
F1 (SS3)	200	1.1×10^{-3}	(363)	(363)	0.0	<0.05
F2 (SS3)	29	1.1×10^{-3}	531	533	0.07	0.07

[a] Strain to necking (uniform elongation measured after occurrence of yield drop)

Table 4. Tensile test results on copper alloy specimens from HFIR-MFE-400J capsule. The tensile data in parentheses are considered unreliable due to bent or brittle tensile specimens.

Alloy, ID Number	Temperature (°C)	Strain Rate (s^{-1})	Yield Strength (MPa)	Ultimate Strength (MPa)	Uniform Elong. (%)	Total Elong. (%)
pure copper, as wrought						
A9 (SS1)—bent/twisted	400	$0.21\text{->}4.2\times10^{-4}$	($\Delta\sigma$~10)	–	–	–
A10 (SS1)-badly bent	400	4.2×10^{-4}	(75)	(113)	(4.7)	(6.1)
GlidCop AL25, as wrought						
H4 (SS1)	400	4.2×10^{-4}	172	190	0.8	9.9
H6 (SS1)	30	4.2×10^{-4}	408	447	5.9	9.1
H5 (SS1)-badly bent	400	$0.21\text{->}4.2\times10^{-4}$	($\Delta\sigma$~7.3)	–	–	–
GlidCop AL15+B, as wr't						
L6 (SS1)	400	4.2×10^{-4}	196	211	1.2	2.5
L7 (SS1)-bent	400	4.2×10^{-4}	(205)	(245)	(2.5)	(5.1)
GlidCop AL25, 50%CW						
X4 (SS3)	400	1.1×10^{-3}	237	273	1.5	10.5
X5 (SS3)	30	1.1×10^{-3}	427	469	8.8	16.2
X6 (SS3)	400	$0.56\text{->}11\times10^{-4}$	$\Delta\sigma$=25.5	219/245	–	–

Table 4 (cont'd). Tensile test results on copper alloy specimens from HFIR-MFE-400J capsule. The tensile data in parentheses are considered unreliable due to bent or brittle tensile specimens.

Alloy, ID Number	Temperature (°C)	Strain Rate (s^{-1})	Yield Strength (MPa)	Ultimate Strength (MPa)	Uniform Elong. (%)	Total Elong. (%)
GlidCop AL25+B, 80% CW						
C6 (SS3)	400	1.1×10^{-3}	300	325	1.0	4.0
C7 (SS3)	400	5.6×10^{-5}	256	280	1.3	1.8
C8 (SS3)	30	1.1×10^{-3}	476	527	7.2	11.5
GlidCop AL25+B, as-wr't						
W4 (SS3)	400	1.1×10^{-3}	201	216	1.0	12.8
W5 (SS3)	400	1.1×10^{-3}	201	225	1.2	11.5
W6 (SS3)	30	1.1×10^{-3}	392	454	8.8	17.2
MAGT 0.2, 50%CW						
T4 (SS3)	400	1.1×10^{-3}	314	328	0.8	5.8
T5 (SS3)	30	1.1×10^{-3}	474	521	8.8	16.2
T6 (SS3)	400	$0.56\text{->}11\times10^{-4}$	$\Delta\sigma$=16.2	310/326	–	–
GlidCop AL15+B, ind. braze						
F5 (SS3)	400	1.1×10^{-3}	(149)	(149)	0.0	<0.05
F6 (SS3)	29	1.1×10^{-3}	(214)	(214)	0.0	<0.05

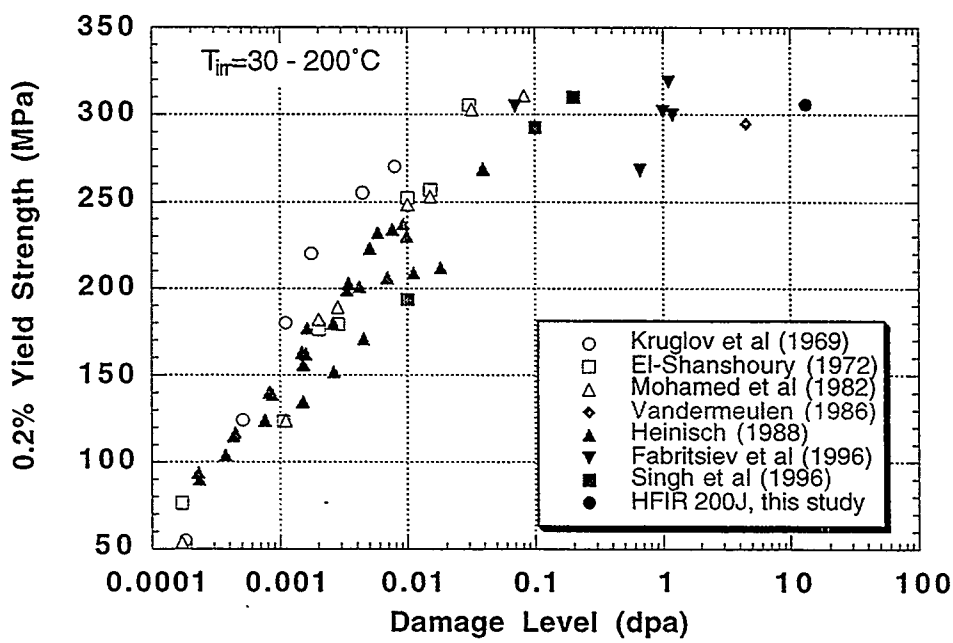

Fig. 1. Dose dependence of radiation hardening in copper irradiated with neutrons at 20-200°C and tested near room temperature [18-24].

An estimate of the barrier strength to dislocation motion can be obtained from a comparison of the radiation-induced defect microstructures [17] and tensile property changes. Figure 2 shows the engineering load-elongation tensile curves for pure copper irradiated at 200°C and tested at room temperature and 200°C (specimens A6 and A8). Using the well-known dispersed barrier hardening equation [25,26] with a Taylor factor of M=3.06 (valid for uniaxial tensile tests on FCC metals [26,27]), the dislocation barrier strength of the defect clusters is estimated to be α=0.15 at

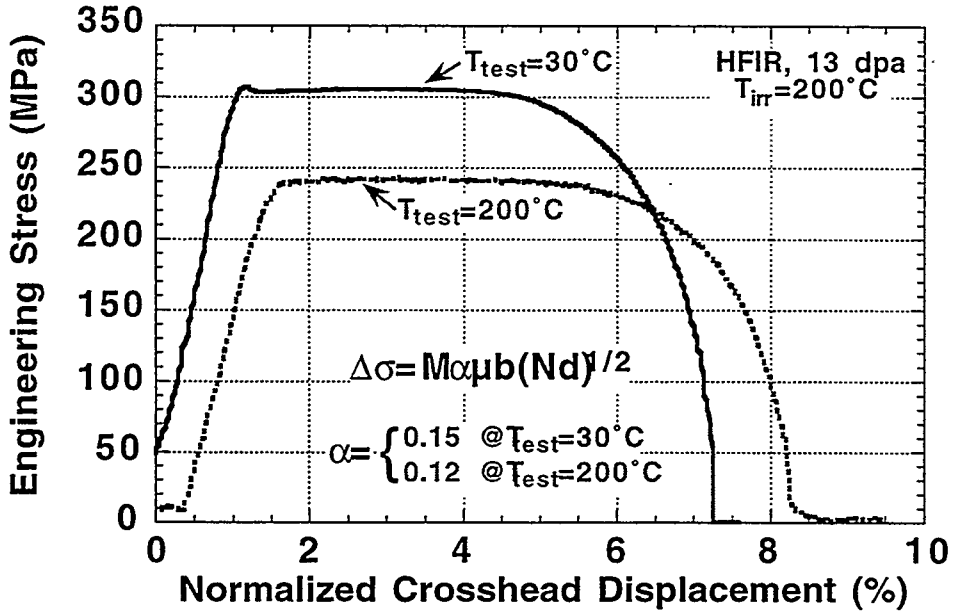

Fig. 2. Uniaxial load-elongation curves for pure copper irradiated to ~13 dpa at 200°C and tested at 30 and 200°C (specimens A6 and A8).

room temperature and 0.12 at 200°C. This result is in agreement with previous estimates obtained on copper irradiated at room temperature to significantly lower doses [26,28]. It is worth noting that a small yield drop was observed in the 200J copper specimen tested at room temperature, whereas a yield drop was not observed in the specimen tested at 200°C.

Figure 3 shows the effect of test temperature on the load-elongation curves of as-wrought GlidCop Al25+B irradiated at 200°C (specimens W1 and W2). There was no clear evidence for a yield drop at either test temperature. From a comparison of Figs. 2 and 3, it is apparent that the irradiated GlidCop Al25 specimens in the HFIR-200J capsule exhibited a steeper test temperature dependence of the yield and ultimate strengths compared to pure copper. The room temperature yield strength of as-wrought GlidCop Al25 was ~550 MPa, which is about 230 MPa higher than the unirradiated value. The corresponding radiation-induced increase in the yield strength at a test temperature of 200°C was ~170 MPa. Therefore, the temperature dependence of the yield strength was more pronounced in irradiated GlidCop Al25 compared to unirradiated specimens.

Figure 4 compares the load-elongation curves of GlidCop Al15 irradiated in the HFIR-200J capsule and tested at 200°C at three different strain rates. The yield strength increased by ~60 MPa and the ultimate tensile strength increased by ~70 MPa as the strain rate was increased by a factor of 500. The initial ("elastic modulus") slope of the stress-strain curves increased with increasing strain rate, which implies that the specimen grip load train system has visco-elastic behavior. There was no significant effect of strain rate on the tensile elongations.

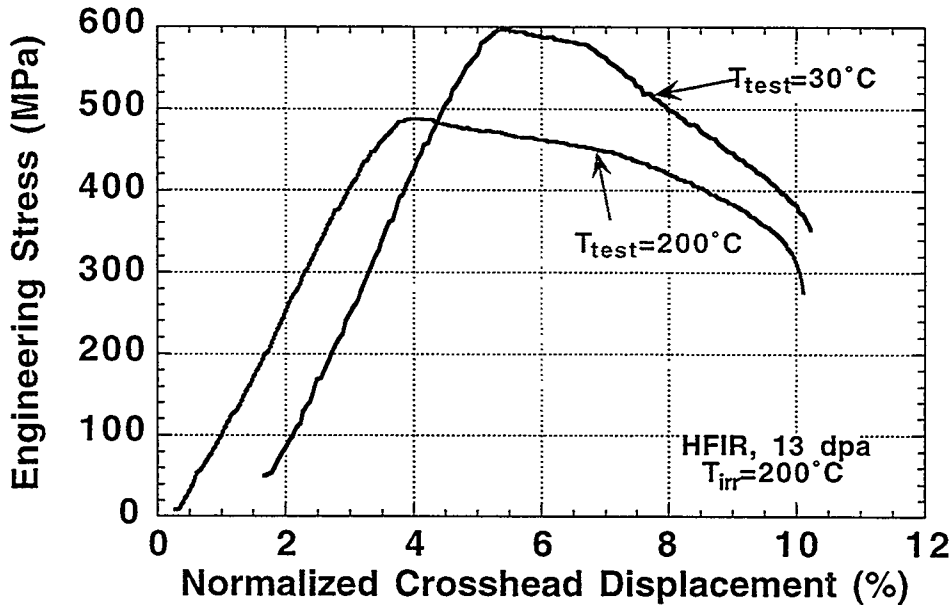

Fig. 3. Uniaxial load-elongation curves for GlidCop Al25+B irradiated to ~13 dpa at 200°C and tested at 30 and 200°C (specimens W1 and W2).

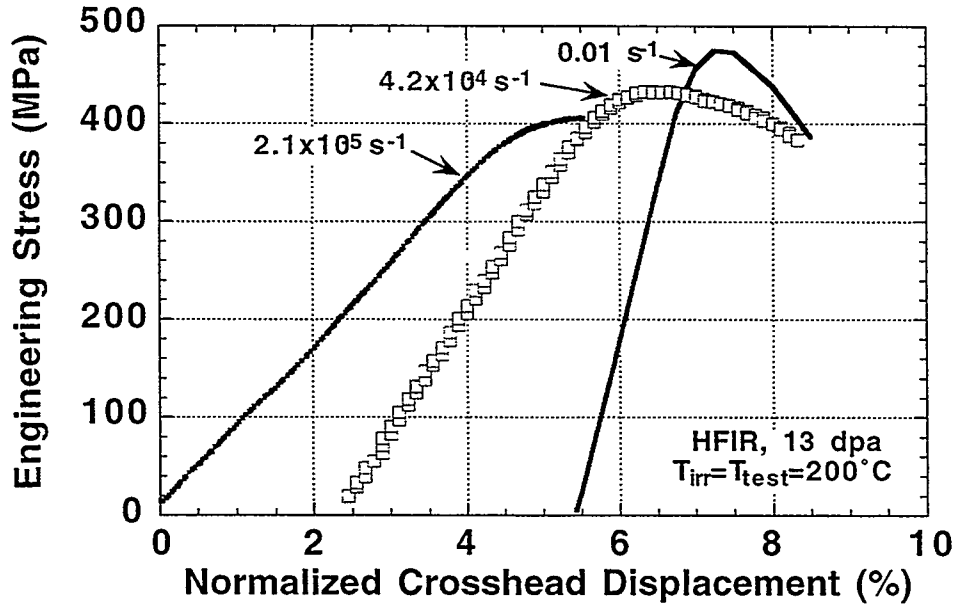

Fig. 4. Uniaxial load-elongation curves for GlidCop Al15+B irradiated to ~13 dpa at 200°C and tested at 200°C at three different strain rates (specimens L1, L2 and L3).

Figure 5 shows the results of a prompt change in strain rate on the load-elongation curve for MAGT 0.2 dispersion strengthened copper irradiated in the HFIR 200J capsule and tested at 200°C (specimen T1). Increasing the strain rate by a factor of twenty produced a small (~16 MPa) increase in tensile strength. The test was performed on a specimen that was bent during capsule disassembly. The bent specimens from the HFIR-200J and –400J capsules were used only for strain rate jump tests, since the deformation produced during capsule disassembly would produce an anomalous and uncontrollable increase in strength. The ~1 to 2% straining prior to the change in strain rate should enable qualitative trends on strain rate sensitivity to be examined in these bent samples. The quantitative accuracy of the strain rate results obtained on the bent samples is uncertain. The ultimate strength measured after the strain rate jump was in good agreement with the value obtained on specimens tested at a constant strain rate of 1.1×10^{-3} s^{-1} (specimens T2 and T2, cf. Table 3).

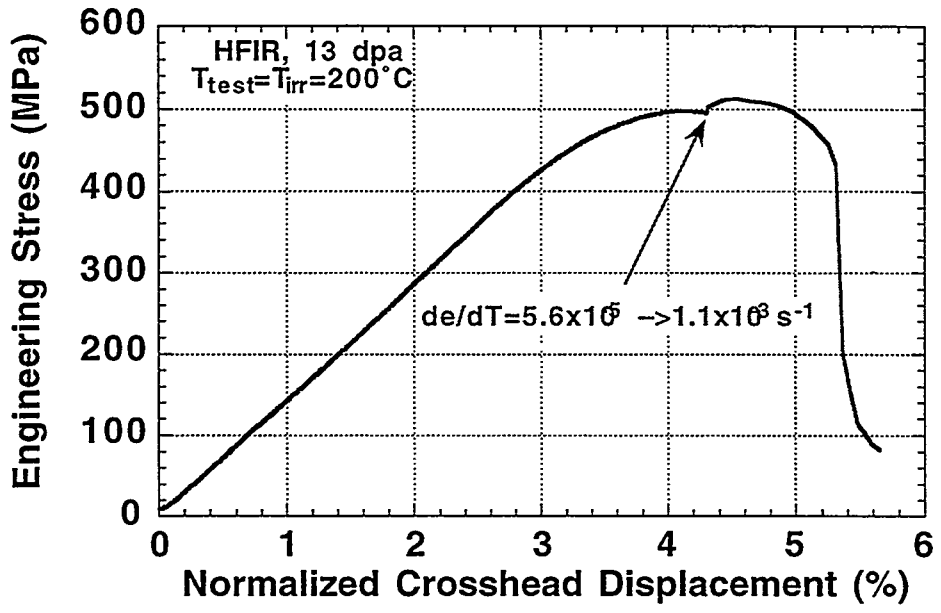

Fig. 5. Effect of increase in strain rate on the uniaxial load-elongation curve for MAGT 0.2 irradiated to ~13 dpa at 200°C and tested at 200°C (specimen T1).

The magnitude of radiation hardening was less pronounced for specimens irradiated at 400°C compared to the 200°C irradiations. For example, the room temperature ultimate strength of wrought GlidCop Al25 was ~580 MPa for the HFIR-200J capsule and ~450 MPa for the HFIR-400J capsule. Figure 6 shows the effect of test temperature on the tensile behavior of GlidCop Al25 irradiated at 400°C (specimens W5, W6). The yield and ultimate strengths varied by a factor of two for the two test temperatures. The radiation-induced increase in yield strength was ~25 MPa at 400°C and ~80 MPa at room temperature. Therefore, both the 200°C and 400°C irradiations resulted in a steeper dependence of yield strength on test temperature compared to unirradiated GlidCop Al25.

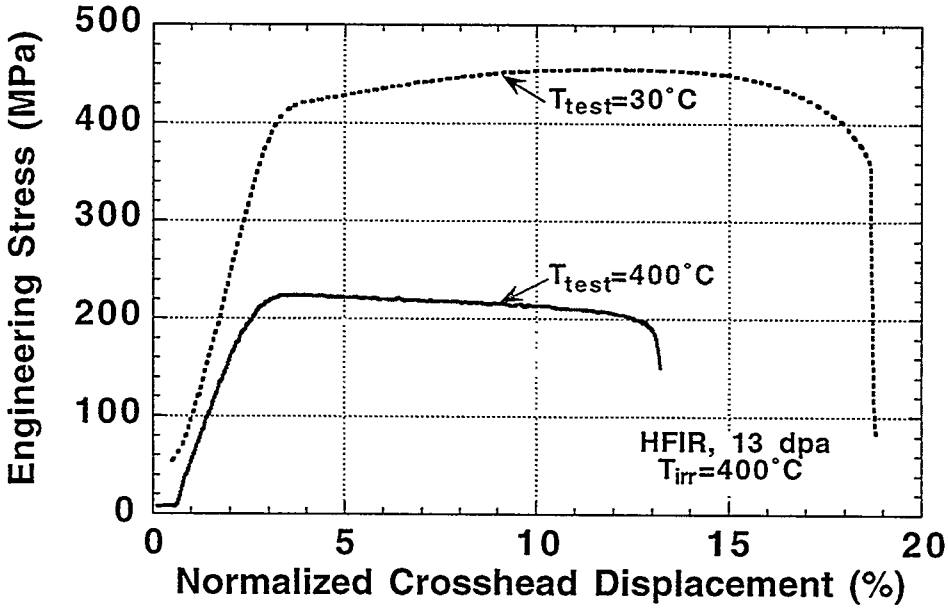

Fig. 6. Uniaxial load-elongation curves for GlidCop Al25+B irradiated to ~13 dpa at 400°C and tested at 30 and 400°C (specimens W5 and W6).

Figure 7 shows the effect of a change in strain rate on the load-elongation curve for 50% cold-worked GlidCop Al25 that was irradiated and tested at 400°C (specimen X6). The factor of 20 increase in strain rate produced an ~25 MPa increase in strength. It is interesting to note that the ultimate tensile strength after the change in strain rate was lower than that of a companion 50% cold-worked GlidCop Al25 specimen tested at a constant strain rate of 1.1×10^{-3} s^{-1} (specimen X4, cf. Table 4). Additional work is needed to determine whether testing of GlidCop Al25 at a slow strain rte at 400°C occurs by a different deformation mode (e.g., grain boundary sliding) compared to faster strain rates, and whether this deformation mode continues to operate if the strain rate is changed during tensile testing (are the results of the strain rate jump test affected by the deformation processes occurring prior to the change in strain rate?).

Figure 8 shows the effect of a factor of twenty increase in strain rate on the load-elongation curve of MAGT 0.2 irradiated and tested at 400°C (specimen T6). The magnitude of the strength increase associated with the change in strain rate (16 MPa) was less than observed for GlidCop Al25 irradiated and tested at the same conditions (Fig. 7). The ultimate strength following the change in strain rate was similar to that obtained from a companion specimen tested at a constant strain rate of 1.1×10^{-3} s^{-1} (specimen T4, cf. Table 4).

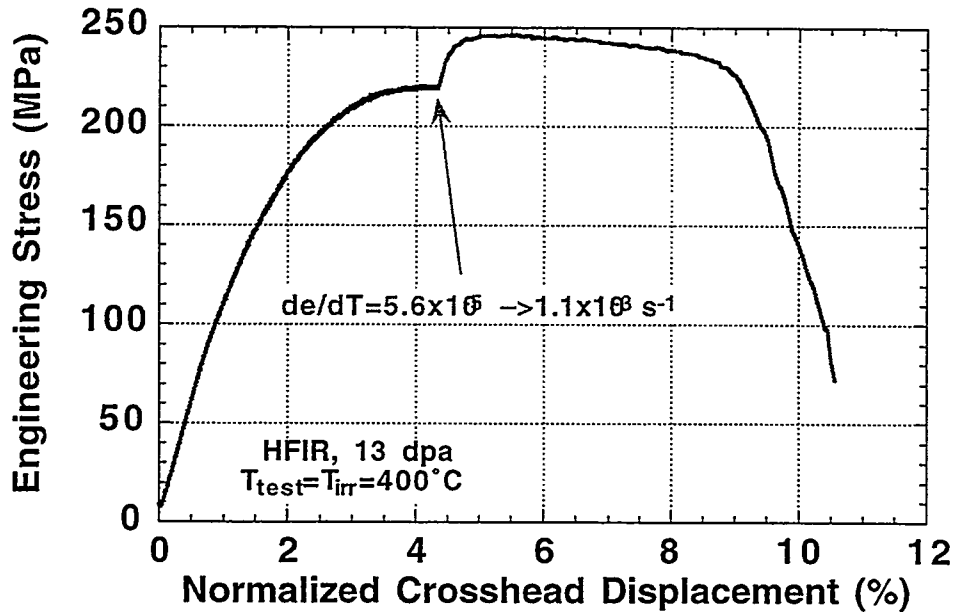

Fig. 7. Effect of increase in strain rate on the uniaxial load-elongation curve for 50% cold-worked GlidCop Al25 irradiated to ~13 dpa at 400°C and tested at 400°C (specimen X6).

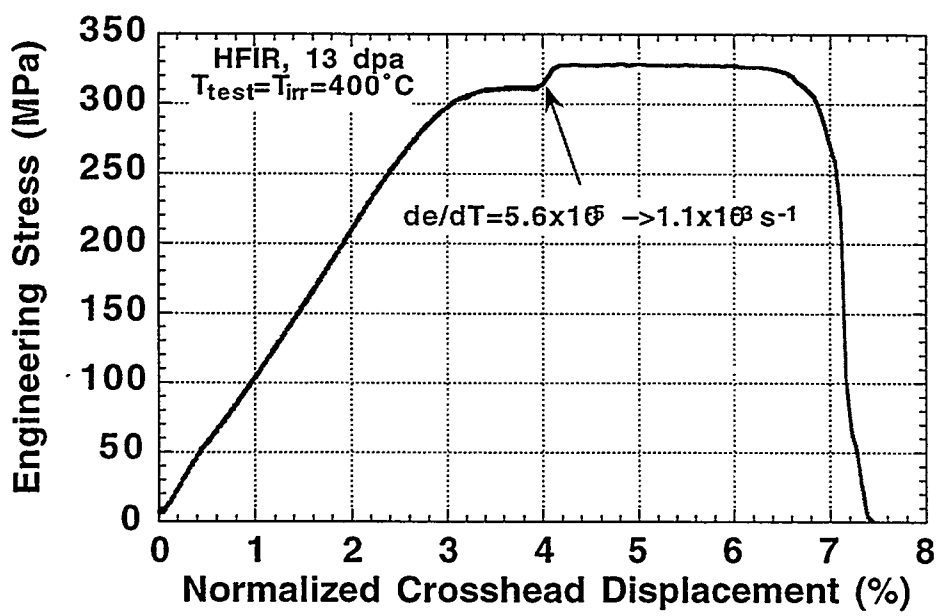

Fig. 8. Effect of increase in strain rate on the uniaxial load-elongation curve for MAGT 0.2 irradiated to ~13 dpa at 400°C and tested at 400°C (specimen T6).

Acknowledgements

The 50% cold-worked sheet of GlidCop Al25 was supplied by F.A. Garner (PNNL), and the remaining GlidCop Al25 (with and without boron) were supplied in rod form by B.N. Singh (Risø). The wrought GlidCop Al25 rod was provided by Bachu Singh via Frank Garner. The MAGT 0.2 sheet was supplied by V.R. Barabash (Efremov Inst.). Auburn University (B.A. Chin) performed the induction brazing of the GlidCop Al15 specimens. The authors thank J.E. Pawel-Robertson for coordinating the specimen insertion and recovery from the HFIR MFE-200J and -400J capsules.

REFERENCES

1. S.J. Zinkle and S.A. Fabritsiev, Atomic and Plasma-Material Interaction Data for Fusion (supplement to Nuclear Fusion) 5 (1994) 163.
2. S.A. Fabritsiev, S.J. Zinkle and B.N. Singh, J. Nucl. Mater. 233-237 (1996) 127.
3. G.M. Kalinin and R. Matera, J. Nucl. Mater. 258-263 (1998) 345.
4. F.A. Garner et al., J. Nucl. Mater. 191-194 (1992) 386.
5. D.J. Edwards et al., J. Nucl. Mater. 191-194 (1992) 416.
6. D.J. Edwards, F.A. Garner, J.W. Newkirk and A. Nadkarni, J. Nucl. Mater. 212-215 (1994) 1313.
7. S.J. Zinkle et al., J. Nucl. Mater. 208 (1994) 119.
8. A.W. Longest et al., in Fusion Materials Semiannual Progress Report for Period ending Sept. 30, 1993, DOE/ER-0313/15 (Oak Ridge National Lab, 1993) p. 23.
9. L.R. Greenwood and C.A. Baldwin, in Fusion Materials Semiann. Prog Rep. for period ending Dec. 31 1997, DOE/ER-0313/23 (Oak Ridge National Lab, 1997) p. 329.
10. A.W. Longest et al., in Fusion Materials Semiannual Progress Report for Period ending March 31, 1993, DOE/ER-0313/14 (Oak Ridge National Lab, 1993) p. 14.
11. S.J. Zinkle and W.S. Eatherly, in Fusion Materials Semiannual Progress Report for Period ending June 30, 1996, DOE/ER-0313/20 (Oak Ridge National Lab, 1996) p. 207.
12. S.J. Zinkle and W.S. Eatherly, in Fusion Materials Semiannual Progress Report for Period ending Dec. 31, 1996, DOE/ER-0313/21 (Oak Ridge National Lab, 1996) p. 165.
13. S.A. Fabritsiev et al., J. Nucl. Mater. 233-237 (1996) 526.
14. S.A. Fabritsiev and A.S. Pokrovsky, J. Nucl. Mater. 249 (1997) 250.
15. D.J. Edwards, F.A. Garner and L.R. Greenwood, J. Nucl. Mater. 212-215 (1994) 404.
16. B.N. Singh, D.J. Edwards and P. Toft, J. Nucl. Mater. 249 (1996) 1.
17. S.J. Zinkle and B.N. Singh, Proc. ICFRM-9, to be published in J. Nucl. Mater. (2000).
18. A.S. Kruglov, V.N. Bykov, I. El-Shanshuri and K. Gaber, Sov. Atomic Energy 26 (1969) 582.
19. I.A. El-Shanshoury, J. Nucl. Mater. 45 (1972) 245.
20. H.G. Mohamed, A.M. Hammad and F.H. Hammad, Trans. Indian Inst. Metals 35 (1982) 258.
21. W. Vandermeulen, V. Massaut, J. Van der Velde and W. Hendrix, in 14th Symp. on Fusion Technology (Pergamon Press, New York, 1986) p. 1031.
22. H.L. Heinisch, J. Nucl. Mater. 155-157 (1988) 121.
23. S.A. Fabritsiev, A.S. Pokrovsky, S.J. Zinkle and D.J. Edwards, J. Nucl. Mater. 233-237 (1996) 513.
24. B.N. Singh, D.J. Edwards and P. Toft, J. Nucl. Mater. 238 (1996) 244.
25. A.L. Bement, Jr., in 2nd Int. Conf. on Strength of Metals and Alloys vol. II, ed. W.C. Leslie (Am. Society for Metals, Metals Park, OH, 1970) p. 693.
26. S.J. Zinkle, Radiat. Eff. Def. Solids 148 (1999) 447.
27. U.F. Kocks, Metall. Trans. 1 (1970) 1121.
28. S. Kojima, S.J. Zinkle and H.L. Heinisch, J. Nucl. Mater. 179-181 (1991) 982.